Available online at www.sciencedirect.com
SCIENCE DIRECT®
PERGAMON
International Journal of Heat and Mass Transfer 46 (2003) 4393–4401
International Journal of HEAT and MASS TRANSFER
www.elsevier.com/locate/ijhmt

Fluid flow and heat transfer model for high-speed rotating heat pipes

F. Song, D. Ewing, C.Y. Ching *

Department of Mechanical Engineering, McMaster University, Hamilton, Ont., Canada, L8S 4L7

Received 7 October 2002; received in revised form 17 May 2003

Abstract

A new complete model has been developed to predict the performance of high-speed rotating heat pipes with centrifugal accelerations up to 10 000 g. The flow and heat transfer in the condenser is modeled using a conventional modified Nusselt film condensation approach. The heat transfer in the evaporator has previously been modeled using a modified Nusselt film evaporation approach. It was found, however, that natural convection in the liquid film becomes more significant at higher accelerations and larger fluid loadings. A simplified evaporation model including the mixed convection is developed and coupled with the film condensation model. The predictions of the model are in reasonable agreement with existing experimental data. The effects of working fluid loading, rotational speed, and pipe geometry on the heat pipe performance are reported here.

1. Introduction

Rotating heat pipes are highly effective two-phase heat transfer devices that can be used for thermal management in a range of rotating systems or machinery, including high-speed drills, electric motors, or compressors [1–3]. Recently, there has been increased interest in using rotating heat pipes in aero-engine applications, where the rotational speeds can exceed 30 000 rpm [4]. A rotating heat pipe, like all heat pipes and thermosyphons, transfers heat by evaporating the working fluid in the evaporator and condensing the vapor at the cooler condenser end. The flow of the working fluid in rotating heat pipes is mainly driven by the centrifugal force imposed by the rotation of the pipe about its axis. Hence, the heat transfer rate of the device is significantly affected by the rotational speed or more properly the centrifugal acceleration.

At low rotational speeds, the liquid flow in a horizontal rotating heat pipe is only partially annular due to gravity, and becomes fully annular only at centrifugal accelerations greater than about 20 g [5]. For a cylindrical rotating heat pipe, the centrifugal acceleration imposed by the rotation is perpendicular to the direction of fluid flow and there must be a decrease in the film thickness in the flow direction to produce a favorable pressure gradient to drive the liquid back to the evaporator. This causes a large film thickness in the condenser reducing the efficiency of the film condensation process [6]. The heat transfer is often enhanced by adding an internal taper in the condenser, and in some cases the evaporator, which utilizes the component of centrifugal force in the axial direction to reduce the film thickness in the condenser.

There has been considerable interest in developing models for the performance of rotating heat pipes in order to optimize their design. The early investigations focused on predicting the condenser performance using a modified Nusselt-type film condensation model [7–10]. The heat transfer in the evaporator was either neglected by arguing that the thermal resistance in the evaporator in the nucleate boiling regime was much less than that in the condenser, or approximated using empirical correlations for pool boiling under acceleration [11]. It was found that the predictions from the model were in reasonable agreement with measurements [8]. Most of these investigations have focused on low and moderate-speed

* Corresponding author. Tel.: +1-905-525-9140; fax: +1-905-572-7944.
E-mail address: chingcy@mcmaster.ca (C.Y. Ching).

0017-9310/$ - see front matter © 2003 Elsevier Ltd. All rights reserved.
doi:10.1016/S0017-9310(03)00292-8

Nomenclature

C_f	skin friction coefficient
C_p	specific heat at constant pressure [$Jkg^{-1}\,K^{-1}$]
g	gravitational acceleration [ms^{-2}]
Gr	Grashof number, $\omega^2 r\cos\alpha\beta\Delta T\delta^3/v_l^2$
h	heat transfer coefficient [$Wm^{-2}\,K^{-1}$]
h_{fg}	latent heat [Jkg^{-1}]
k	heat conductivity [$Wm^{-1}\,K^{-1}$]
L	heat pipe length [m]
$\dot{m}$	mass flow rate [kgs^{-1}]
Nu	Nusselt number, $h\delta/k_l$
P	pressure [Pa]
Pr	Prandtl number, v/α
q	heat flux [Wm^{-2}]
Q	heat transfer rate [W]
r	local radius [m]
R	heat pipe radius [m]
R_l	liquid film thermal resistance [K/W]
Ra	Rayleigh number, $GrPr$
Re	liquid film Reynolds number, $4u_l\delta/v_l$
T	temperature [K]
u	velocity [ms^{-1}]
U	liquid velocity at the liquid–vapor interface [ms^{-1}]
α	taper angle [°]
δ	liquid film thickness [m]
μ	dynamic viscosity [$kgm^{-1}\,s^{-1}$]
v	kinematic viscosity [$m^2\,s^{-1}$]
ρ	density [kgm^{-3}]
τ	shear stress [Nm^{-2}]
ω	angular velocity [$rads^{-1}$]

Subscripts

c	condenser
e	evaporator
f	forced convection
i	inner side
l	liquid
m	mixed convection
n	natural convection
o	outer side
sat	saturation
v	vapour
w	wall
δ	liquid–vapor interface

(<3000 rpm) rotating heat pipes with typical centrifugal accelerations less than 200 g. Ponnappan et al. [12] recently measured the heat transfer rates of heat pipes at rotational speeds from 10 000 to 30 000 rpm with accelerations in the range 1000–9600 g. The heat transfer performance of the condenser predicted using the modified Nusselt film condensation model was more than an order of magnitude larger than their measurements. They also found that the heat transfer performance of the condenser decreased with rotational speed, which was contrary to the predictions from the model. As a result they stated that the previous condensation model did not capture all of the physics of high-speed rotating heat pipes.

It should be noted that the effect of fluid loading could not be included into the previous condensation models for rotating heat pipes since the models did not include the complete cycle of the working fluid. In practical applications, the heat pipes are charged with an excess amount of the working fluid in order to prevent local dryout in the evaporator. For example, the fluid loading in the experiments of Ponnappan et al. [12] is up to 15 times the ideal fluid loading. Li et al. [13] noted that the effect of fluid loading could be initially examined using a simple film evaporation model for the evaporator that was analogous to the modified Nusselt film condensation model used in the condenser. They used this to complete the model of the heat pipe and found that the performance of the condenser was, in fact, adversely affected by increasing the fluid loading. In particular, although the excess fluid tends to pool in the evaporator of a tapered rotating heat pipe, it increases the liquid film thickness in the condenser at high fluid loadings. It should be noted that both the condensation model [8] and the combined film condensation/evaporation model [13] evaluated the heat transfer performance of the heat pipe by examining the heat transfer in the condenser as a function of the temperature difference between the vapor and the condenser wall rather than the temperature difference across the heat pipe. Hence, these results can only be used to predict the performance of rotating heat pipes if the thermal resistance of the evaporator is negligible.

Generally, nucleate boiling is suppressed within the liquid film in the evaporator as the centrifugal acceleration increases [14–17]. Although the exact transitional acceleration is not known, nucleate boiling is completely suppressed at about 600 g [15]. Under these conditions, the phase transformation in the evaporator may occur by film evaporation at the liquid surface [11], which is generally applicable for rotating heat pipes at low rotational speeds (accelerations), or at high rotational speeds with high-thermal-conductivity metal working fluids. Song et al. [6] used this model to predict the

performance of rotating heat pipes of different geometries including a cylindrical pipe under accelerations up to 1100 g. In high-speed rotating heat pipes with common working fluids such as water and methanol, natural convection within the liquid film is enhanced in the evaporator compared to conduction heat transfer across the liquid film. In this case, previous closed-form analytical solutions are not sufficient to describe the heat transfer processes in the evaporator. Song et al. [18] noted that the natural convection in the liquid film due to the centrifugal acceleration became more important as the fluid loading was increased, causing the liquid to pool in the evaporator. They introduced a mixed convection model to account for the effect of natural convection in the presence of high acceleration and large fluid loading.

A new complete model for the high-speed rotating heat pipe is presented in this paper. Following Li et al. [13] the solutions for the liquid flow and heat transfer in the condenser, the adiabatic section, and the evaporator are coupled so that the model can predict the performance of rotating heat pipes with either ideal or non-ideal fluid loadings. The performance of the condenser is modeled using the conventional modified Nusselt film condensation approach, while the performance of the evaporator is modeled using a film evaporation approach that includes correlations for both natural and mixed convection. The model was validated by comparisons with the experimental data of Ponnappan et al. [12]. The effects of both design and operating parameters on a rotating heat pipe with rotational speed ranging from 10 000 to 30 000 rpm are presented.

2. Rotating heat pipe model

2.1. Governing equations

A rotating heat pipe (Fig. 1) consists of three sections: a condenser, an adiabatic section, and an evaporator. The models for each section are coupled together to obtain the overall heat transfer performance of the heat pipe as a one-domain problem. The momentum equations of the thin-film liquid flow at steady state are

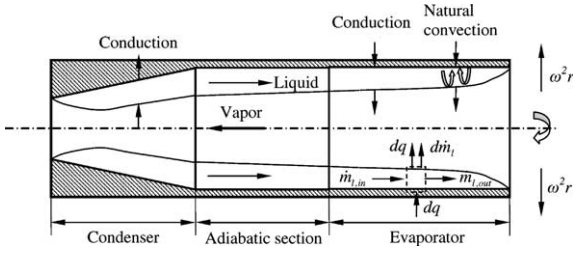

Fig. 1. Schematic of rotating heat pipe.

$$\rho_l \omega^2 r \sin\alpha - \frac{\partial P_l}{\partial x} + \frac{\partial \tau_l}{\partial y} = \rho_l u_l \frac{\partial u_l}{\partial x} \tag{1}$$

$$\rho_l \omega^2 r \cos\alpha + \frac{\partial P_l}{\partial y} = 0 \tag{2}$$

Neglecting heat conduction along the axial direction, the energy equations for the liquid flow and heat pipe walls are

$$k_l \frac{\partial^2 T}{\partial y^2} = \rho_l C_{pl} u_l \frac{\partial T}{\partial x} \tag{3}$$

$$k_w \frac{\partial^2 T}{\partial y^2} = 0 \tag{4}$$

Assuming a smooth liquid–vapor interface with negligible surface tension effects and 1-D vapor flow, the boundary conditions at the wall and liquid–vapor interface are

$$x = 0 \quad \text{and} \quad x = L: \quad \dot{m}_l = 0 \tag{5}$$

$$y = 0: \quad u_l = 0 \quad \text{and} \quad -k_l \frac{\partial T}{\partial y} = q_w \tag{6}$$

$$y = \delta: \quad P_{l,\delta} = P_{v,\delta} = P_{sat} \quad \text{and} \quad T = T_{sat} \tag{7}$$

$$\tau_{l,\delta} = \mu_l \frac{\partial u_l}{\partial y} = \frac{d\dot{m}_l}{dx}(u_v \cos\alpha + u_{l,\delta}) - \tau_{v,\delta} \cos\alpha \tag{8}$$

2.2. Film condensation/evaporation model

A film evaporation model analogous to the modified Nusselt film condensation model can be used to complete the model for rotating heat pipes if both nucleate boiling and natural convection are absent in the evaporator. The liquid inertia term in the flow direction in Eq. (1) is of the second order in magnitude compared with the force terms and can be neglected. This was subsequently confirmed through numerical simulations using the integral momentum equation. Integration of Eq. (2) with the assumption that the local radius r in the liquid flow is equal to R_i due to the very thin film yields

$$P_l = P_{sat} + \rho_l \omega^2 R_i \cos\alpha(\delta - y) \tag{9}$$

The liquid velocity is obtained by substituting Eq. (9) into Eq. (1) and integrating it twice with respect to y

$$\begin{aligned} u_l = {} & \frac{\rho_l}{\mu_l}\omega^2 R_i \left(\sin\alpha - \cos\alpha \frac{d\delta}{dx}\right)\left(y\delta - \frac{y^2}{2}\right) \\ & - \frac{y}{\mu_l}\frac{d\dot{m}_l}{dx}(u_v \cos\alpha + u_{l,\delta}) + \frac{1}{\mu_l}\frac{\partial P_v}{\partial x}\left(\frac{y^2}{2} - y\delta\right) \\ & - \frac{y\tau_{v,\delta}}{\mu_l}\cos\alpha \end{aligned} \tag{10}$$

The four terms on the right of Eq. (10) correspond to the effects of the sum of centrifugal force and hydrostatic pressure variation in the liquid flow direction,

momentum change at the interface due to phase transformation, vapor pressure drop, and vapor shear force at the interface. The hydrostatic pressure gradient term is often neglected in previous models but retained here so that the model can be applied to the cylindrical heat pipe. To evaluate the vapor effects, two non-dimensional ratios R_1 and R_2 are estimated based on a 1-D vapor flow.

$$R_1 = \frac{\tau_{v,\delta}}{\rho_l \omega^2 r\left(\sin\alpha - \cos\alpha \frac{d\delta}{dx}\right)\delta} \quad \text{and}$$
$$R_2 = \frac{\Delta P_v / L}{\rho_l \omega^2 r\left(\sin\alpha - \cos\alpha \frac{d\delta}{dx}\right)} \tag{11}$$

R_1 and R_2 represent the ratio of vapor shear stress at the interface and pressure gradient to the liquid driving force, respectively. The interfacial shear stress is calculated using the Blasius equation and the pressure gradient is estimated from the Bernoulli equation. For $\omega^2 r > 1000$ g, the typical values of R_1 and R_2 are less than 0.001 and hence the vapor effects are neglected by dropping the corresponding terms.

For any control volume in the liquid film (Fig. 1), the mass conservation can be written as

$$\dot{m}_{l,in} = \dot{m}_{l,out} + d\dot{m}_l \tag{12}$$

where the liquid mass flow rate at the cross section is given by

$$\dot{m}_l = \int_0^\delta 2\pi r \rho_l u_l \, dy \tag{13}$$

Heat transfer across the liquid film is simplified by assuming conduction only and neglecting the second-order convection term in Eq. (3).

$$k_l \frac{\partial^2 T}{\partial y^2} = 0 \tag{14}$$

The heat flux through the heat pipe inner wall and liquid film is balanced by the phase change at the liquid–vapor interface.

$$q_w = \frac{k_w (T_{w,i} - T_{w,o})}{R_i \ln(R_o/R_i)} \tag{15}$$

$$q_l = q_w = k_l (T_{sat} - T_{w,i})/\delta = h_{fg} d\dot{m}_l / (2\pi R_i \, dx) \tag{16}$$

The film condensation/evaporation model can be solved by coupling the liquid flow Eqs. (10)–(13) and heat transfer Eqs. (15) and (16). The liquid flow in the adiabatic section is similar to that in the condenser, but with no heat transfer.

2.3. Mixed convection evaporator model

At high accelerations ($\omega^2 r > 1000$ g) and low heat flux ($q < 200$ kW/m^2), nucleate boiling is suppressed and natural convection becomes dominant in the liquid film in the evaporator. Under these conditions, the liquid velocity profile depends on whether the flow is laminar or turbulent. In a boundary layer, the flow transitions from laminar to turbulent as the Ra number increases. The velocity profile for a turbulent boundary layer can be approximated by a 1/7th power law. The velocity profile predicted as a function of K ($K = Gr/Re^{5/2}$) for mixed convection over a horizontal plate [19] agrees well with this trend. In this instance, the velocity profile in the presence of mixed convection is approximated by a power law where the magnitude of the power depends on whether forced or natural convection dominates and if the flow is laminar or turbulent.

$$\frac{u_l}{U} = \left(\frac{y}{\delta}\right)^b$$
$$\text{where } \begin{cases} b = 1/3 & \text{when } 1 < Gr/Re^2 < 10, \ Ra < 10^9 \\ b = 1/4 & \text{when } Gr/Re^2 > 10, \ Ra < 10^9 \\ b = 1/7 & \text{when } Ra \geqslant 10^9 \end{cases} \tag{17}$$

The unknowns U and δ are determined from Eq. (12) and the integral momentum equation

$$\int_0^\delta \omega^2 r\left(\sin\alpha - \cos\alpha \frac{d\delta}{dx}\right) dy - \frac{\tau_w}{\rho_l} - \frac{\tau_{v,\delta}}{\rho_l}$$
$$= \frac{d}{dx}\int_0^\delta u_l (u_l - U)\, dy + \frac{dU}{dx}\int_0^\delta u_l \, dy \tag{18}$$

where $\tau_{v,\delta} = C_{f,\delta} \rho_v u_v^2/2$ and $\tau_w = C_{f,w} \rho_l U^2/2$, in which $C_{f,\delta}$ is determined by the Blasius equation and $C_{f,w}$ using the results of Afzal and Hussain [20] for mixed convection over a horizontal plate

$$C_{f,w} = \begin{cases} 0.5 & (0 < K \leqslant 1) \\ 0.5K^{3/5} & (K > 1) \end{cases} \tag{19}$$

The mixed convection heat transfer in the liquid film is modeled by the correlation for mixed convection in a forced horizontal boundary layer with a transverse buoyancy force [21]

$$q_l = h_m (T_{w,i} - T_{sat}) = (Nu_m k_l/\delta)\Delta T \tag{20}$$

$$Nu_m^{7/2} = Nu_f^{7/2} + Nu_n^{7/2} \tag{21}$$

The forced convection is approximated using the modified Nusselt film evaporation model. In the case of low Reynolds number liquid flow, $Nu_f = 1$. Several empirical correlations have been recommended for natural convection under acceleration [11], in which the heat transfer rate is proportional to $(\omega^2 r)^a$ where $0.25 < a < 0.375$. The correlation by Korner reported by Marto [11] was adopted here for the natural convection induced by acceleration.

$$Nu_n = 0.133 Ra^{0.375} \tag{22}$$

2.4. Calculation scheme

The heat pipe is discretized into finite control volumes along its axial length. The film condensation model

(Eqs. (10)–(16)) and mixed evaporation model (Eqs. (17)–(22)), with the appropriate boundary conditions (Eqs. (5)–(8)), are solved iteratively for each control volume to ensure conservation of mass and energy. In the presence of excess fluid loading, the liquid film thickness at the evaporator end cap is initially assumed and the film thickness profile along the heat pipe is solved for numerically. The fluid loading is calculated and the evaporator end cap film thickness is changed till the loading approaches the given fluid loading. The grid is subsequently refined till results independent of the grid size are obtained.

2.5. Model validation

The current model for high-speed rotating heat pipes was verified by simulating the test cases examined experimentally by Ponnappan et al. [12]. It should be noted that the heat pipe tested by Ponnappan et al. [12] was charged with about 15 times the ideal fluid loading, where ideal fluid loading (100%) is defined as the fluid mass in the heat pipe such that the film thickness at the evaporator end cap is zero for a given rotational speed. The current model results for the heat transfer rate with the temperature difference across the liquid film in the condenser ΔT_c are in good agreement with the experimental data for rotational speeds in the range 10 000 to 30 000 rpm (Fig. 2). The Nusselt condensation model [8] significantly over predicts the experimental data (Fig. 2), since the model can not take into account the redistribution of the excess fluid throughout the pipe due to the high fluid loading. As the fluid loading increases, the liquid film thickness in the condenser becomes thicker with a consequent decrease of the conduction heat transfer across the film. Both previous models and the current model predict an increase of heat transfer with the rotational speed, which is opposite to that of the experimental data, the reasons for which are not known at this point.

In the current model, the liquid velocity profile is assumed based on physical arguments. A sensitivity analysis of the assumed velocity profile was performed to examine its influence on the accuracy of the model results. The heat transfer rates for different values of the exponent b (in Eq. (17)) were evaluated at 10 000 rpm and were found to be nearly identical, with a maximum error of 2% at ideal fluid loading. The choice of b affects the liquid film thickness distribution along the evaporator. The natural convection along the evaporator length, however, is enhanced with an increase in liquid film thickness resulting in almost a constant heat transfer in the evaporator for different values of b. For the case of very low fluid loadings, the contribution from natural convection is negligible and in this case the heat transfer is affected slightly by the choice of b. It can be concluded that the choice of b in the liquid velocity profile has a negligible effect on the prediction of overall heat pipe performance, particularly for overcharged fluid loadings.

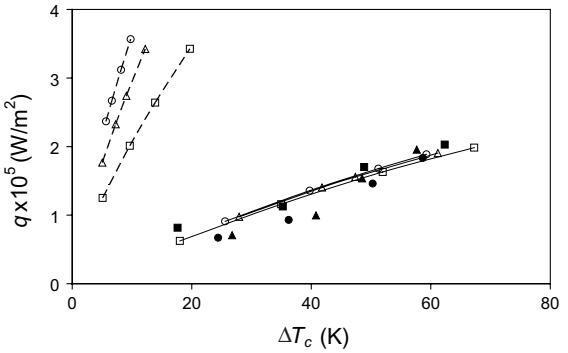

Fig. 2. Comparison between model predictions and experimental results [12]. ——, current model and – – –, Nusselt model at □, 10 000 rpm; △, 20 000 rpm; ○, 30 000 rpm with experimental data at the same speed represented by solid symbols.

3. Results and discussion

The effects of fluid loading, rotational speed and taper geometry on the heat pipe performance were investigated using the present model. A constant wall temperature of 100 and 60 °C on the outside of the evaporator and condenser were used for the simulations. For consistency, the rotating heat pipe studied here has the same nominal dimensions (Table 1) as that tested by Ponnappan et al. [12].

3.1. Effect of fluid loading

The effect of fluid loading on the flow and heat transfer characteristics within the liquid film was initially investigated at 10 000 rpm using a 1° condenser taper. The ideal fluid loading (100%) is about 0.007 kg in this instance, which is defined as the fluid loading that gives a zero film thickness at the evaporator end cap. It is determined by solving for the liquid film thickness profile as well as the vapor flow through the heat pipe. The ideal fluid loading is significantly affected by the

Table 1
Nominal dimensions of rotating heat pipe

Length of evaporator/adiabatic/ condenser	0.076/0.057/ 0.089 m
OD-pipe wall (stainless steel)	0.0254 m
ID-evaporator	0.0191 m
ID-condenser	0.016/0.0191 m
Adiabatic section taper angle	0°
Working fluid	Water

rotational speed since the increase in acceleration and centrifugal driving force is beneficial for the liquid return from the condenser to the evaporator, reducing the film thickness in the condenser. It is also influenced by heat pipe geometry, where a taper structure can lead to thinner liquid films and consequently less amount of working fluid.

The liquid film thickness (δ/D) distribution along the heat pipe for fluid loadings from 100% to 1000% are presented in Fig. 3. For the ideal fluid loading case, δ/D increases along the flow direction in the tapered condenser due to the increase in condensate mass flow rate. The centrifugal driving force due to the taper ($\rho_l\omega^2 r\sin\alpha$) in the condenser section results in a much thinner liquid film than that in the cylindrical adiabatic and evaporator sections. A hydraulic jump occurs with a sudden increase in δ/D near the intersection between the tapered condenser and cylindrical adiabatic sections due to the sudden change in section geometry. The hydrostatic pressure gradient drives the liquid back through the cylindrical adiabatic and evaporator sections and the film thickness reduces in the flow direction until it reaches the evaporator end cap. As the fluid loading increases, most of the excess liquid pools at the adiabatic and evaporator sections, with the film surface being relatively flat in these two sections. The film thickness in the condenser increases with the fluid loading, but retains its general shape.

Increasing the fluid loading reduces the heat transfer in the condenser due to the increase in liquid film thickness. In the evaporator, although the conduction heat transfer is reduced due to the thicker liquid films, the natural convection in the liquid film is enhanced. The relative importance of natural and forced convection in the evaporator can be estimated from the magnitude of the local Gr/Re^2 (Fig. 4). For a given fluid loading, Gr/Re^2 increases along the flow direction and reaches a maximum at the evaporator end cap ($x/L = 1$), with the exception of the ideal fluid loading case. The increase of local Gr/Re^2 along the evaporator is mainly due to the decrease in local Re as the velocity decreases to zero at the evaporator end cap. The magnitude of Gr remains relatively constant along the evaporator in this case since there is no significant change in liquid film thickness. For ideal fluid loading, however, the liquid film thickness reduces to zero at the evaporator end cap. As a result, the magnitude of Gr decreases significantly near the end cap with a corresponding decrease in Gr/Re^2. For ideal fluid loading, $Gr/Re^2 \approx 0.1$ indicating dominant forced convection in the evaporator. With an increase of fluid loading, the average Gr/Re^2 in the evaporator increases and mixed convection and eventually natural convection dominates in the evaporator.

The development of natural convection enhances the heat transfer in the liquid film and influences the wall superheat $\Delta T_{sat,w}$ in the evaporator (Fig. 5). Here, $\Delta T_{sat,w} = T_{w,i} - T_{sat,w}$, where $T_{sat,w}$ is calculated based on the hydrostatic pressure due to the centrifugal acceleration. The contribution of acceleration to $T_{sat,w}$ is, however, very small due to the very thin liquid films. For the case of ideal fluid loading, conduction heat transfer dominates for small values of Gr/Re^2 and $\Delta T_{sat,w}$ decreases along the flow direction with the decrease of liquid film thickness. For the case of excess fluid loading, $\Delta T_{sat,w}$ remains nearly constant due to the relatively flat liquid surface in the evaporator. As the fluid loading increases, natural convection becomes more dominant and $\Delta T_{sat,w}$ reduces, which contributes to the suppression of nucleate boiling. At a fluid loading of 1000%, $\Delta T_{sat,w}$ is lower than that for ideal fluid loading in the upstream region of the evaporator, although the liquid film is much thicker than the ideal fluid loading case. This is mainly due to the higher heat transfer by natural convection in the liquid film for the excess fluid loading case.

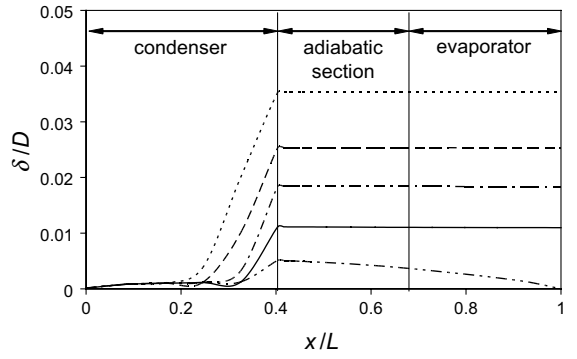

Fig. 3. Variation of liquid film thickness distribution at 10 000 rpm and fluid loadings of – - -, 100%; ——, 300%; – –, 500%; ———, 700%; - - - -, 1000%.

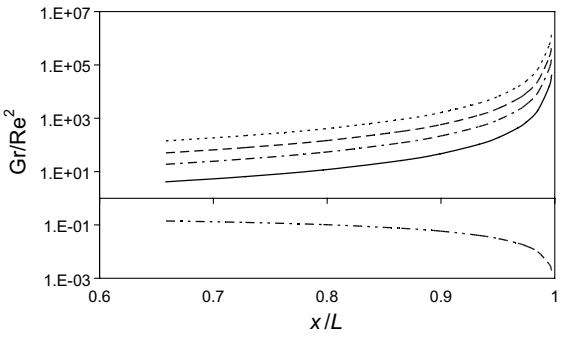

Fig. 4. Variation of Gr/Re^2 distribution in the evaporator at 10 000 rpm and fluid loadings of – - -, 100%; ——, 300%; – –, 500%; ———, 700%; - - - -, 1000%.

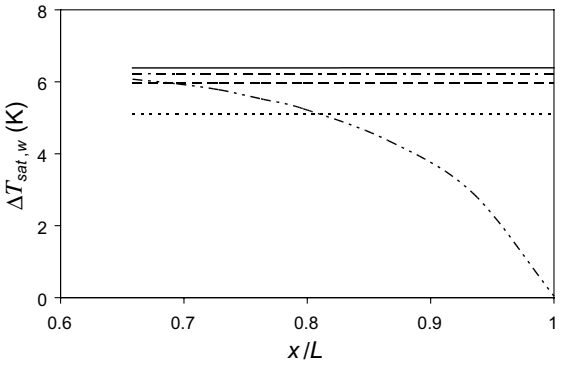

Fig. 5. Distribution of wall superheat in the evaporator at 10 000 rpm and fluid loadings of – - - -, 100%; ——, 300%; – – –, 500%; ———, 700%; - - - -, 1000%.

3.2. Effect of rotational speed

The rotational speed or acceleration affects the liquid flow through the variation of centrifugal driving force and hydrostatic pressure within the liquid film. The variation of the liquid film thickness distribution with rotational speed for a given fluid loading (100% at 10 000 rpm) is shown in Fig. 6. In the condenser, the liquid film thickness decreases as the rotational speed increases due to the larger centrifugal driving force, with the excess liquid pooling at the evaporator end. Since the hydrostatic pressure force $(\rho_l \omega^2 r \frac{d\delta}{dx})$ drives the liquid back to the evaporator in the cylindrical sections, an increase of rotational speed $(\omega^2 r)$ results in smaller $(\frac{d\delta}{dx})$ of the liquid film profile in the adiabatic and evaporator sections. The redistribution of the liquid film has a significant influence on the overall heat transfer characteristics of the heat pipe. In the condenser, conduction heat transfer is increased due to the thinner liquid films, while the dominant heat transfer mode in the evaporator

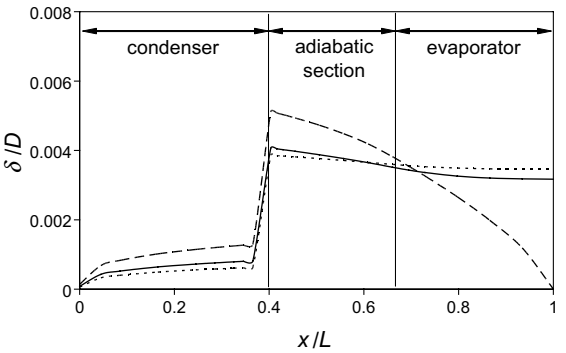

Fig. 6. Change in the liquid film thickness variation for rotational speeds of – – –, 10 000 rpm; ——, 20 000 rpm; - - - -, 30 000 rpm.

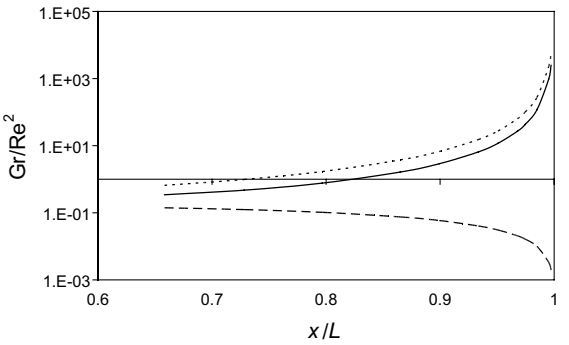

Fig. 7. Variation of Gr/Re^2 distribution in the evaporator for rotational speeds of – – –, 10 000 rpm; ——, 20 000 rpm; - - - -, 30 000 rpm.

changes from forced convection to mixed convection and finally natural convection as the rotational speed increases. This is reflected in the distribution of Gr/Re^2 in the evaporator, where the average Gr/Re^2 increases from 0.1 to several hundred as the rotational speed increases from 10 000 to 30 000 rpm (Fig. 7). The variation of $\Delta T_{sat,w}$ along the evaporator length (Fig. 8) is similar to the variation of liquid film thickness, where $\Delta T_{sat,w}$ decreases as the rotational speed increases due to the enhancement in natural convection heat transfer with speed.

3.3. Heat transfer performance

The effects of fluid loading and rotational speed on the overall heat transfer performance are shown in Fig. 9. For the same fluid loading, the heat transfer increases by about 10% as the rotational speed increases from 10 000 to 30 000 rpm. This is smaller than that found for the low and moderate-speed range, where the heat transfer rate was found to be approximately proportional to the square root of rotational speed [6]. This difference can be attributed to the variation of film thickness in the condenser with rotational speed. As the speed increases, the film thickness decreases more significantly in the low-speed range than at the high-speed range, resulting in a smaller effect of speed on the heat transfer at higher rotational speeds. For a given rotational speed, the heat transfer rate reduces as the fluid loading increases mainly due to an increase in the thermal resistance in the condenser. The evaporator thermal resistance, however, remains nearly constant with fluid loading due to the enhancement of natural convection. This can be further analyzed by examining the thermal resistance of liquid film R_l in the condenser and evaporator (Fig. 10). In the condenser, there is a continuous increase in R_l with fluid loading due to an increase in film thickness. The R_l in the evaporator, on the other hand, remains relatively constant with fluid loading because

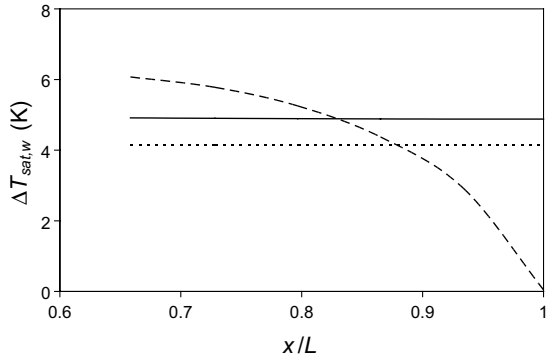

Fig. 8. Distribution of wall superheat in the evaporator for rotational speeds of – – –, 10 000 rpm; ——, 20 000 rpm; - - - -, 30 000 rpm.

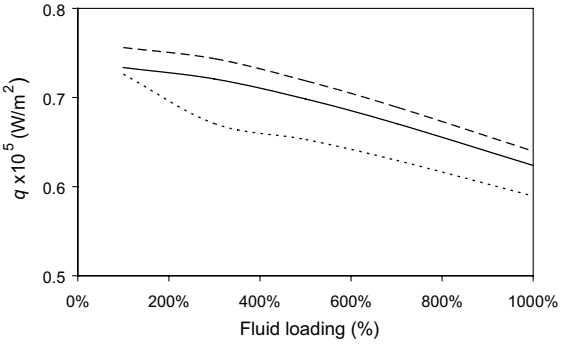

Fig. 9. Heat transfer performance for different fluid loadings and rotational speeds - - - -, 10 000 rpm; ——, 20 000 rpm; – – –, 30 000 rpm.

the increase in liquid film thickness is offset by an increase in natural convection. The R_l in the evaporator is comparable to that in the condenser up to a fluid loading of about 700%, indicating that the evaporator can have a significant effect on the overall heat pipe performance at these fluid loadings. At very high fluid loadings, the effect of the evaporator heat transfer to the overall heat pipe performance decreases. However, the evaporator needs to be included in the model since it affects the distribution of the liquid film thickness in the condenser. For a given fluid loading, the R_l in both the condenser and evaporator decreases with an increase in rotational speed, with the decrease being much less prominent at higher rotational rates.

3.4. Effect of heat pipe geometry

For the heat pipe with fixed outer diameter, the effect of a taper in the condenser and evaporator on the overall heat pipe performance is presented in Fig. 11 for a given fluid mass charge. With no taper in the evaporator, the heat transfer initially increases with an increase in condenser taper angle and then decreases after a peak value at $\alpha_c \approx 0.3°$. The condensate flow rate increases with taper angle due to the increased centrifugal driving force with resultant thinner liquid films and higher heat transfer. However, as the taper is increased, the available internal heat transfer area for a given heat pipe outer diameter decreases. At small taper angles, the enhancement of heat transfer is greater than the reduction due to the decrease in surface area and the overall heat transfer increases. As the taper angle increases beyond a critical point, the increase in heat transfer due to the thinner film in the condenser can not compensate for the reduction of heat transfer surface area due to the taper. The addition of a taper to the evaporator, on the other hand, tends to always reduce the overall heat transfer rate. The taper does not increase the heat transfer in the evaporator significantly, resulting in a decrease in the total heat transfer due to the reduction in surface area.

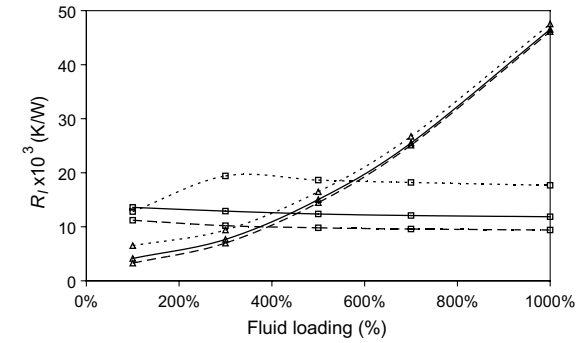

Fig. 10. Comparison of thermal resistance of liquid film in the condenser and evaporator △, condenser; □, evaporator; - - - -, 10 000 rpm; ——, 20 000 rpm; – – –, 30 000 rpm.

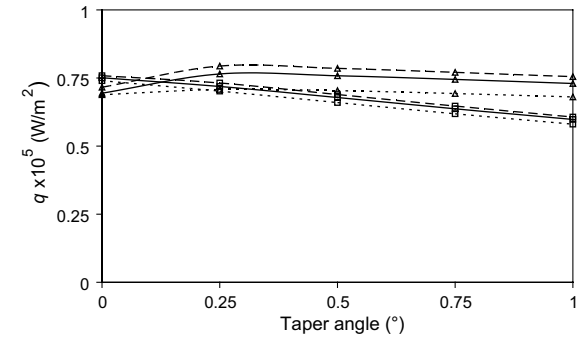

Fig. 11. Effect of condenser and evaporator taper on heat transfer performance △, condenser; □, evaporator; - - - -, 10 000 rpm; ——, 20 000 rpm; – – –, 30 000 rpm.

4. Conclusions

A new complete model for high-speed rotating heat pipes with centrifugal accelerations up to 10 000 g has been developed. The modified Nusselt film condensation model for the condenser is coupled with an evaporation model and the overall heat transfer is solved for as a one-domain problem. In the evaporator, mixed and natural convection dominates at high accelerations and are incorporated in the evaporator model. The model predictions are in good agreement with existing experimental data at high rotational speeds. The effect of fluid loading and rotational speed on the heat pipe performance was investigated using the current model. As the fluid loading increases, the overall heat pipe performance decreases mainly due to the increase of film thickness in the condenser. The fluid loading does not significantly affect the heat transfer at the evaporator even though the films are thicker because of the increase in natural convection with film thickness. There is an increase in heat transfer with rotational speed, with the increase being smaller than that observed at lower rotational speeds. The liquid film thermal resistance in the evaporator is comparable to that in the condenser and plays an important role in the overall heat pipe performance. For a rotating heat pipe with a given outer diameter, an optimum condenser taper exists to obtain the maximum overall heat transfer. The inclusion of a taper in the evaporator, however, decreases the overall heat transfer since the taper does not play a significant role in the evaporator heat transfer.

Acknowledgements

The support of the Natural Sciences and Engineering Research Council (NSERC) of Canada and Pratt & Whitney Canada is gratefully acknowledged. The authors would also like to acknowledge the many helpful discussions with R. Judd, M. Dowhan and J. Brand.

References

[1] V.H. Gray, The rotating heat pipe—A wickless hollow shaft for transferring high heat fluxes, ASME No. 69-HT-19, 1969.
[2] O. Oslejsek, F. Polasek, Cooling of electrical machines by heat pipes, in: Proceedings of Second International Heat Pipe Conference, Italy, 1976, pp. 503–514.
[3] R. Ponnappan, J.E. Leland, Rotating heat pipe for high speed motor/generator cooling, SAE 981287, 1998, pp. 257–262.
[4] R. Ponnappan, J.E. Leland, High speed rotating heat pipe for aircraft applications, SAE 951437, in: Aerospace Atlantic Conf., Dayton, OH, 1995.
[5] G.P. Peterson, An introduction to heat pipes, John Wiley & Sons, Inc., New York, 1994.
[6] F. Song, C.Y. Ching, D. Ewing, Fluid flow and heat transfer modeling in rotating heat pipes, in: Twelfth International Heat Transfer Conference, Grenoble, France, 2002.
[7] P.J. Marto, Laminar film condensation on the inside of slender, rotating truncated cones, J. Heat Transfer 95 (1973) 270–272.
[8] T.C. Daniels, F.K. Al-Jumaily, Investigation of the factors affecting the performance of a rotating heat pipe, Int. J. Heat Mass Transfer 18 (1975) 961–973.
[9] T.C. Daniels, R.J. Williams, The effect of external boundary conditions on condensation heat transfer in rotating heat pipes, Int. J. Heat Mass Transfer 22 (1979) 1237–1241.
[10] A. Faghri, Heat pipe science and technology, Taylor & Francis, Washington, DC, 1995.
[11] P.J. Marto, Rotating heat pipes, in: D.E. Metzger, N.H. Afgan (Eds.), Heat and Mass Transfer in Rotating Machinery, Hemisphere Publishing Co., 1984, pp. 609–632.
[12] R. Ponnappan, Q. He, J.E. Leland, Test results of a high speed rotating heat pipe, AIAA Paper No. 97-2543, 1997.
[13] H.M. Li, C.Y. Liu, M. Damodaran, Analytical study of the flow and heat transfer in a rotating heat pipe, Heat Recover. Syst. CHP 63 (2) (1993) 115–122.
[14] H. Merte, J.A. Clark, Pool boiling in an accelerating system, J. Heat Transfer 83 (1961) 233–242.
[15] J.C. Eschweiler, A.M. Benton, G.W. Prechshot, Boiling and convective heat transfer at high accelerations, in: Chemical Engineering Progress Symposium Series, vol. 63 (79), 1967, pp. 66–72.
[16] R.L. Judd, H. Merte Jr., Evaluation of nucleate boiling heat flux predictions at varying levels of subcooling and acceleration, Int. J. Heat Mass Transfer 15 (1972) 1075–1096.
[17] M.E. Ulucakli, H. Merte Jr., Nucleate boiling with high gravity and large subcooling, J. Heat Transfer 112 (1990) 451–457.
[18] F. Song, D. Ewing, C.Y. Ching, Effects of evaporator design on the performance of rotating heat pipes, in: Canadian Society for Mechanical Engineering Forum, Kingston, 2002.
[19] W. Schneider, A similarity solution for combined forced and free convection flow over a horizontal plate, Int. J. Heat Mass Transfer 22 (1979) 1401–1406.
[20] N. Afzal, T. Hussain, Mixed convection over a horizontal plate, J. Heat Transfer 106 (1984) 240–241.
[21] S.W. Churchill, Combined free and forced convection around immersed bodies, in: G.F. Hewitt (Ed.), Heat Exchanger Design Handbook, Hemisphere, Washington, DC, 1990.